An Analysis of Radial Cold Spray Nozzles

K. J. Lewis

Department of Physics

Mount Holyoke College

Supervisor

David Schmidt, Department of Mechanical and Industrial Engineering,

University of Massachusetts Amherst

In partial fulfillment of the requirements for the degree of

Bachelor of Arts

May, 2022

Acknowledgements

I am deeply grateful for the help of Prof. David Schmidt during the course of this research. His guidance was invaluable. I came in knowing nothing about cold spray and came out knowing at least a small amount. I am also thankful for the other members of my committee, Prof. Kathy Aidala and Prof. Spencer Smith, for supporting me throughout my undergraduate career.

I would like to acknowledge the help of the other members of my lab for all their support. I'd particularly like to thank Sampath Rachakonda for helping me get my simulations working when they refused to work and for helping me get my thoughts down on paper when I didn't know what to say. Thank you all for helping me troubleshoot when nothing was working and getting excited when it finally did.

Thank you to my parents for everything they've done for me and their continuous support. Thank you for late-night phone calls and sudden trips to campus when I was feeling down. Thank you (and apologies) to my siblings for enduring my endless rambling about cold spray. I know you didn't understand a word, but thank you for humoring me.

Thank you Prof. Jason Young and the rest of the MHC Astrophysics Lab. I learned so much about how to conduct collaborative research from the semesters I spent with you all. I've loved seeing what you've all been up to since I left.

Thank you to the Mount Holyoke Department of Physics. I'm so grateful to have been a part of this community, and I'm so proud of all of my fellow students. Your research projects are fascinating and ground-breaking, and I can't wait to see where you all go from here.

Abstract

Cold spraying, also known as gas dynamic cold spraying or supersonic particle deposition, is an additive manufacturing technique wherein powder particles are accelerated by a carrier or driving gas passing through a supersonic nozzle and impinged on a substrate. Powders used in cold spray range from a metal, alloy, polymer, or composite powder material. In the past this technique has primarily been used to form protective coatings for surfaces, but the process is also used for the repair and restoration of damaged or worn parts, or to machine a part that would be difficult or impossible to otherwise create. Although cold spray has many benefits over similar fabrication and restorative processes due to less heat stress on the substrate, a key concern arises when considering small, internal surfaces. Cold spray relies on the high velocity of the particles—rather than on their temperature—to bond with the substrate. When repairing an internal surface that is too narrow for the full nozzle to fit into, it must be bent to accommodate the smaller diameter. This bend of the nozzle provides an additional surface for the particles to hit, causing either clogging or erosion of the nozzle interior, depending on the impacting particle's velocity. In this project, previous radial cold spray nozzle designs were assessed and compared with revised versions to determine a more optimal design for a radial cold spray nozzle.

Contents

List of Figures

Chapter 1

Introduction

This chapter discusses the present state of cold spray technologies and identifies open questions and then summarizes the work done for this thesis. The second chapter of this paper describes the research methodology and simulation setup. The third chapter describes the results of the simulations and discusses their implications. The fourth chapter recaps the findings and gives recommendations for future studies.

1.1 Background

Cold spraying, also known as gas dynamic cold spraying or supersonic particle deposition [1, 2], is an additive manufacturing technique wherein powder particles are accelerated by a carrier or driving gas passing through a supersonic nozzle and impinged on a substrate. Powders used in cold spray range from a metal, alloy, polymer, or composite powder material. In the past this technique has primarily been used to form protective coatings, but the process is also used for the repair and restoration of damaged or worn parts [2, 3], joining of two dissimilar metals [4], or to fabricate a part that would be difficult or impossible to otherwise machine [5].

An illustrated overview of the cold spray process is given in Fig. 1.1. The particle matter is added to the carrier gas through the powder feeder just prior to the supersonic nozzle, which is where the particles are accelerated to supersonic speed. Once leaving the nozzle, if the particles have reached their critical velocity, they will bond with the substrate through ballistic impingement. Typically, either nitrogen or helium is used as the carrier gas [6]; however, air may also be used [7, 8].

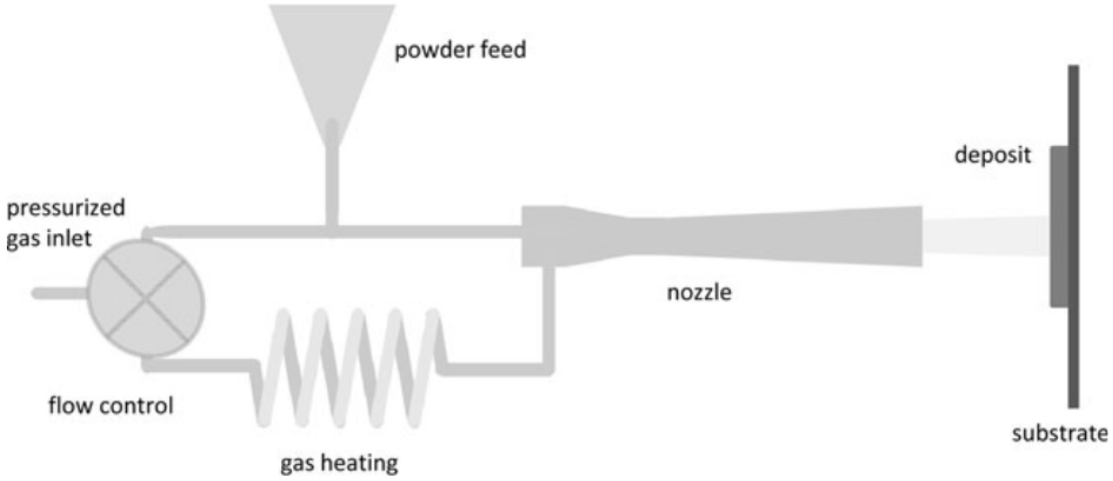

Figure 1.1 Overview of the cold spray process [17]

A key aspect of cold spray is the particles' ability to reach a certain critical velocity. It is only when the spray material reached velocities above the necessary critical velocity that they will be able to successfully deposit on the substrate. Critical velocity depends on the properties of both the spray material and substrate [9, 10]. Major factors affecting the critical velocity necessary for bonding include the yield stress, the strain hardening index, and the particle strength coefficient [10, 11]. The particle velocity, and therefore ability to reach and maintain the critical velocity, is affected by factors including: nozzle expansion ratio, length of the entrance convergent section, driving gas conditions, particle density and size, presence of shock waves, and divergent section length [12, 13]. It is widely believed that particle adhesion is due to adiabatic shear instability [14, 15]; however, some researchers have proposed that this is not necessary for bonding [16].

Cold spray applies a material layer-by-layer at relatively cool temperatures compared to thermal sprays. This is one of its key advantages over thermal sprays and other alternatives such as welding. Unlike thermal spray techniques, the powder is not melted during the spraying process. Rather, the kinetic energy of the particles causes them to undergo plastic deformation at bonding. Due to this process occurring at lower temperatures and without melting the particle matter, coatings may be produced with properties that are unachievable by thermal spray methods [18]. Since cold spray uses comparatively lower temperatures, there is both less heat stress and fewer heat-affected zones. Cold spray also retains the initial chemical and material properties of the material and, due to the

low heat used, is less prone to oxidation [10, 19, 20]. This makes cold spray ideal for coatings involving materials that would otherwise oxidize.

This method produces a hard, high density, cold-worked coating that can range in thickness from several millimeters to several centimeters [19]. Due to compaction, the density of layers closer to the substrate is greater than that of layers farther away from the substrate [20]. The layers placed down initially are compacted by each subsequent layer, progressively getting more compact as layers are added down.

Nozzles of both round and rectangular cross-sections are used in the cold spray process [8, 21]. For the purposes of this study, only round cross-sections are being considered.

The most common nozzle type used in cold spray is a convergent-divergent—or de Laval—nozzle; however, convergent-barrel [22, 23] and convergent-divergent-barrel [20, 22, 23] nozzles are also used to accelerate the spray material. The three barrel designs can be seen in Fig. 1.2. Of these three nozzles, the de Laval nozzle gives the greatest particle velocity upon exiting the nozzle [23]. The convergent-barrel nozzle, on the other hand, gives a smaller velocity but greater temperature compared to the de Laval nozzle; additionally, although the particle velocity in a convergent-barrel nozzle is less than that in a de Laval nozzle, the ratio of particle velocity to gas velocity is higher [24]. It also maintains a constant velocity throughout the barrel section of the nozzle. With a de Laval nozzle, most of the spray particles are accelerated to a velocity greater than the critical velocity with the use of a carrier gas. Compared to thermal spray processes, the gas flow rate is much higher; and, particularly if helium is used, the cost is also relatively high. With the use of a convergent-barrel nozzle, both of those can be reduced.

There are numerous applications of cold spray technologies. These include repairs and restoration, the rapid manufacturing of low-tolerance parts, and the manufacturing of parts that would be awkward or impossible to machine otherwise. Through the use of cold spray, a deposit layer may be produced to even out surfaces and provide a protective coating. This coating can either be put down preemptively to protect a piece of machinery from typical wear and tear, or it can be created after the fact to diminish or erase the effects of prolonged use. This paper will be focused on the applications of wear reduction and repair of damaged components.

1.2 Turning Supersonic Flow

When repairing aircraft or similar machinery, sometimes it is necessary to repair inner surfaces that are awkward or impossible for the cold spray nozzles as-is to fit into. A basic method of adjusting cold spray nozzles for internal coating applications is to simply shorten the nozzle [20]. However, the nozzle can only be shortened so much since the particles must travel through a certain length of nozzle in order to reach their critical velocity. The longer the nozzle length, the greater the particle's velocity upon impact with the substrate; accordingly, if the nozzle length is decreased beyond a certain point, the particles are unable to reach the critical velocity necessary to bond with the substrate. Some of this can be mitigated by using helium instead of nitrogen. Since helium has both a higher specific heat ratio and a higher specific gas constant, it can increase to higher velocities in short nozzles with the same expansion ratio [25].

Other than shortening the nozzle, there are two primary methods for dealing with internal cold spray. Since there was no consistent naming convention used in previous literature, in this thesis they will be referred to as directional and radial nozzles. Directional nozzles, such as in Fig. 1.3, feature the entire nozzle bent into a particular direction. Radial nozzles, such as in Fig. 1.4, which features 360° radial spray to coat all internal surfaces at once.

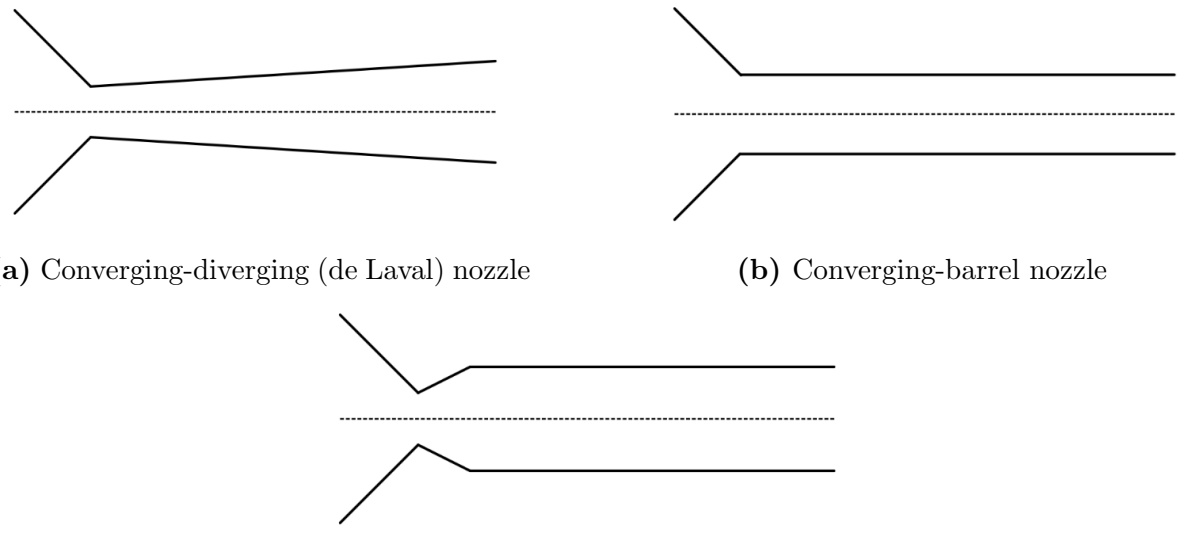

(a) Converging-diverging (de Laval) nozzle

(b) Converging-barrel nozzle

(c) Converging-diverging-barrel nozzle

Figure 1.2 Three main nozzle types used in cold spray. The dotted line indicates the center axis.

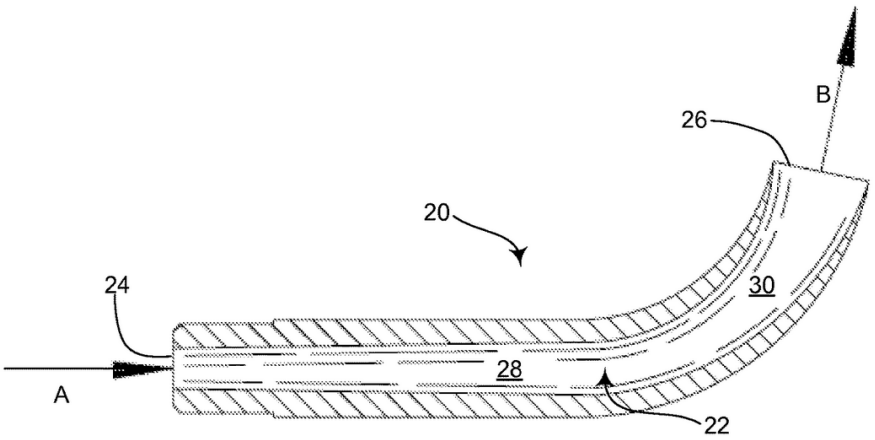

Figure 1.3 Directional cold spray nozzle [26]. Numbering from original.

The first of these nozzle types is directional nozzles [25–27], where the nozzle is bent at an angle to accommodate the smaller area it can fit into. Using either a single nozzle or a set of nozzles, the inner surface of the substrate may be sprayed with a coating. However, this requires either a partial or complete rotation of the treated tube. The nozzles used here can vary from converging-diverging—where the diverging portion of the nozzle continues through both the axial and radial sections of the pipe—and converging-diverging-barrel—where the diverging portion is relegated to the upstream axial section. A key benefit to a continuous diverging section is that without it, the carrier gas and particles experience deceleration throughout the bend, which can impair their ability to maintain the critical velocity necessary to bond with the substrate.

Another alternative is to use a radial nozzle. This nozzle design uses an annular nozzle, such as in Fig. 1.4, to create a 360° spray which avoids the need of rotating either the pipe or spray surface to coat the interior [28–33]. This method is more efficient in coating internal surface of cylindrical tubes, since all sides may be coated at once. It is also a more straightforward coating process than the directional spray method described previously because there is no tube rotation necessary. If radial cold spray nozzles are designed as two plates held together by a center pin, this also provides ease of maintenance as one plate can be removed if necessary. This grants greater access to the interior of the cold spray nozzle.

Important considerations to be made in bent nozzle designs are the severity of the bend angle and the locations of the convergent and divergent sections compared to the

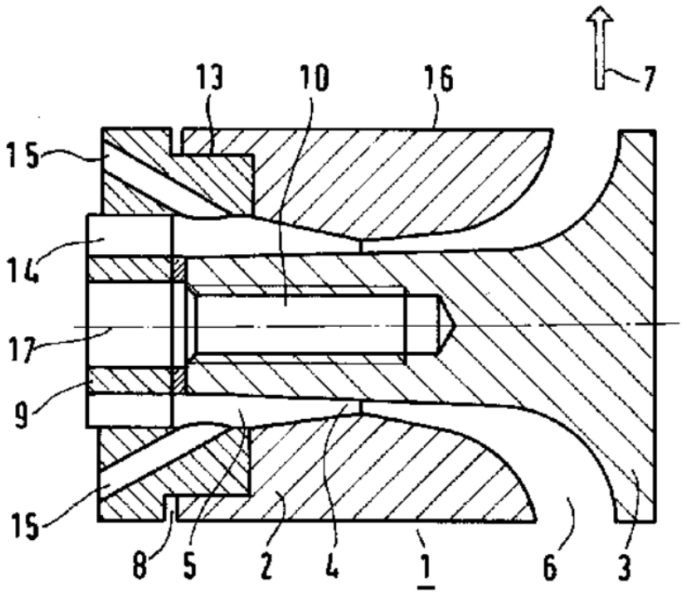

Figure 1.4 Annular cold spray nozzle [28]. Numbering from original.

bend (i.e. whether to use a convergent-divergent or convergent-divergent-barrel nozzle). If the bend is more gradual, the fluid flow will be able to more easily move around the bend without particle powder colliding with the nozzle wall. However, if the nozzle is still bending close to the outlet, the spray material may have reached a high enough velocity that it will be more likely to impinge on the nozzle at said bend and therefore be more likely to clog it.

Although it may not be practical to simply use a shortened nozzle, this necessitates turning the supersonic flow which comes with certain inherent challenges. Turning supersonic flow results in shocks and expansion fans. Additionally, secondary flows occur whenever flow in a pipe encounters a bend [34–37]. Viscous forces cause a velocity gradient, which is normal to the plane of curvature [38, 39]. At the bend, fluid going faster than the average fluid flow speed will move to the outside of the bend; conversely, fluid traveling at a speed less than the average will move to the inside of the bend (see Fig. 1.5). This is due to the presence of radial pressure gradients. A pressure differential forms to balance the centrifugal force on the fluid, with higher pressures occurring at the outer wall and lower pressures occurring at the inner wall [36]. When fluid is pushed to the outer wall, it will slow down due to its proximity to the boundary layer and subsequently be pushed back to the inner wall. Consequently, due to the non-uniform velocity, this constant secondary movement of the flow will cause a diminished flux and greater losses than a corresponding length of straight pipe [35]. As long as secondary velocities are

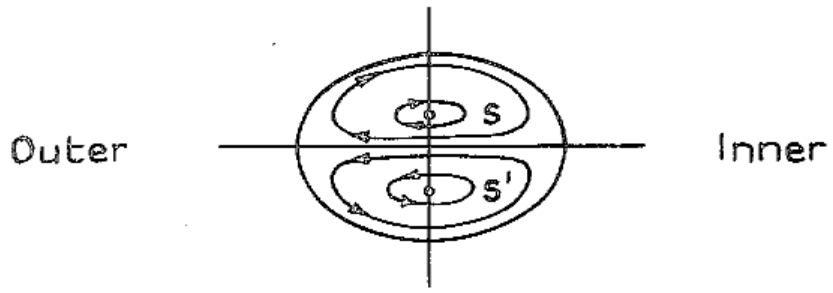

Figure 1.5 Secondary flow in a curved pipe. The fluid flows around two points, labeled S and S' [36].

small, however, the losses due to secondary flow will also remain small [35]. There also may be variable heat transfer rates and the fluid may choke at the bend, which would cause changes in the mass flow rate and a decreased velocity. Strong oscillations in the flow may develop due to the aforementioned secondary flows or due to flow separation.

With a limit on divergent section length, the increased presence of shock waves, and a greater chance of collisions with the angled nozzle wall, a possible issue that may arise in turning supersonic flow is decreased particle velocity. This may impair the powder particles' ability to accelerate to their critical velocity and therefore be less likely to bond with the substrate.

When designing these nozzles, one factor to look at is how uniform the particle distribution is. A recurring problem with cold spray is the resulting microstructural inhomogeneity of the deposit, caused by factors such as variations in particle sizes and velocities [6]. One possibility is that shock waves resulting from turning supersonic flow may result in greater irregularity of the deposit. Other factors to consider are the minimum length of the acceleration section necessary to achieve the critical velocity and the typical length of the supersonic jet, which determine the width of the internal surface that the nozzle will be able to spray.

1.3 Nozzle Clogging and Erosion

A large change in particle direction due to the nozzle bend will lead to increased collisions with the channel wall. This can subsequently lead to one of two outcomes. If the particles continue at or above their critical velocity, they have a chance to bond with the nozzle wall and produce clogging. Conversely, particles that collide with the nozzle before they

have accelerated fast enough to adhere will wear away at the inner wall. Similarly, if the secondary flows, shocks, and expansion fans slow the particles to below their critical velocity, they will erode away the surface of the nozzle upon impact.

Nozzle clogging, or nozzle fouling, occurs when the spray material collides with and adhere to the inner nozzle wall. Clogging is an inherent risk in bent cold spray nozzles due to the change in fluid flow direction. Not all particles will smoothly follow the curve of the nozzle, and some will instead collide with the nozzle wall. As a result of nozzle clogging, the working cross-sectional area of the nozzle decreases. This means that the flow velocity, and the particle exit velocity, are also decreased. Accordingly, there is also a decrease in particle deposition, since the particles may not reach their critical velocity. The nozzle operating window also decreases.

Nozzle fouling is both an expensive and an inconvenient problem. Frequent nozzle replacement is not feasible due to the high expense of nozzle materials. Instead of replacing a clogged nozzle it can be cleaned, but this requires inconvenient machining to remove the particle build-up and restore the nozzle to working condition.

Another possible issue with radial cold spray nozzles is the erosion of the inner nozzle wall. If the particles do not accelerate enough to reach their critical velocity, then they will not bond with the surface they hit. Instead, they will erode away at it. Particles with higher hardness such as tungsten and chromium are more likely to cause erosion and impact damage on the surface of the substrate due to their worse deformation capacity [11]. This makes it difficult to deposit these materials on the substrate.

Whether clogging or erosion of the wall occurs depends on whether or not the powder particles have managed to accelerate to their critical velocity prior to impact. Nozzle clogging and nozzle erosion both alter the cross-sectional area of the nozzle, changing the flow acceleration and resulting particle deposition.

A possible solution to the clogging predicament is to turn the particles at the initial part of the acceleration section, thereby minimizing chances for the particles at their highest velocity to collide with and deposit on the nozzle wall. This was the thinking behind the nozzles developed by Kosarev et al [30]. However, although the particles may not cause clogging of the nozzle interior, since they are moving at lower speeds they will instead wear away at it. Neither of these outcomes is ideal since they both alter the shape of the channel and the flow path.

1.4 Overview

This study looks into radial cold spray designs of the type described by Kosarev et al [30, 31]. This nozzle design features a severe angle of bend. As mentioned previously, a sudden and dramatic turn angle presents a major clogging issue. The 90° bend angle of the nozzle creates a wall obstructing the flow that particles of sufficiently high velocity will impinge upon. On the other hand, if the bend is too early in the flow path and the particles have not accelerated to their critical velocity, they will instead erode away the inner wall surface. The aims of this study are to find a more optimal nozzle design to minimize both clogging and erosion of the nozzle while also optimizing the shape of the nozzle to avoid flow separation

Chapter 2

Methods

2.1 ANSYS FLUENT

For the purposes of this research, simulations were conducted using ANSYS FLUENT v21.2 and v22.1 [40]. Nozzle geometries were either created as CAD files in Autodesk Fusion 360 [41] and imported into ANSYS Workbench or created directly in ANSYS Workbench using ANSYS DesignModeler. They were then used to run 2D axisymmetric simulations.

ANSYS FLUENT is a commercial computational fluid dynamics (CFD) simulation software that uses the finite volume method (FVM) to solve fluid dynamics problems. In addition to the FVM, other prominent solution methods used in CFD are the finite difference (FDM) and finite element (FEM) methods [42]. In all of these methods, illustrated in Fig. 2.1, the flow geometry is divided into smaller components that are then used to solve a particular set of governing equations. However, the various numerical methods differ in how they go about solving the given set of partial differential equations.

The FVM is the most common numerical solution method used by commercially-available CFD simulators [42]. It discretizes a geometry into a computational mesh of contiguous, non-degenerate cells or control volumes. For each of these cells, a set of conservation equations are iteratively solved and then averaged, relying on the fact that what goes into each cell must then come out of that same cell. This process, and the governing equations used by ANSYS FLUENT, are further explained below.

The FDM finds an unknown variable by sampling different points and then generating finite difference approximations of the partial derivatives at each point and its neighboring

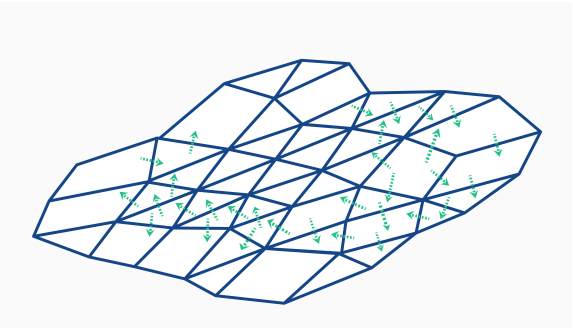

(a) Finite volume method

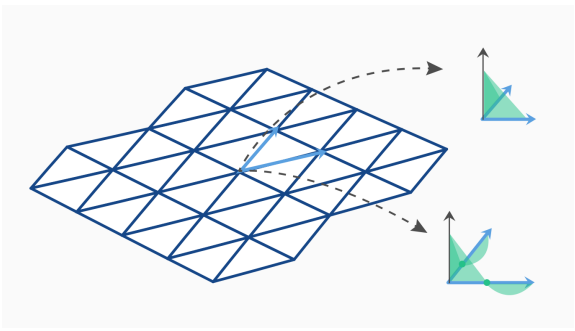

(b) Finite element method

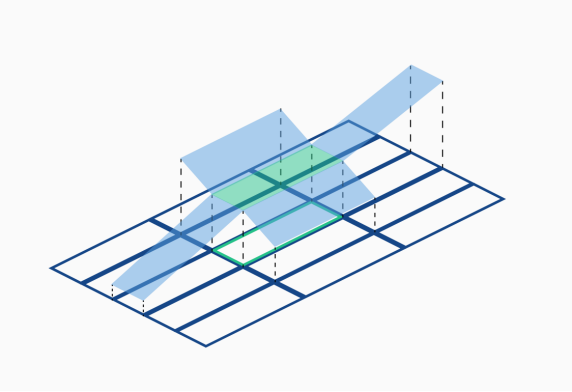

(c) Finite difference method

Figure 2.1 CFD discretization methods [43].

points. These approximations are done through Taylor series expansions. Truncating the Taylor series after a smaller number of terms rather than a larger number decreases the accuracy of the expansion but also decreases the complexity.

In the FEM, the geometry is subdivided into simple geometric shapes, or elements, similar to the control volumes used in the FVM. However, instead of using conservation laws, the FEM uses piecewise polynomial functions to approximate the solution.

ANSYS FLUENT uses five principle governing equations to represent mass, momentum, and energy conservation [40]. There is one equation each for mass and energy conservation, along with three equations for conservation of momentum. These equations are also called the Navier-Stokes equations. Each local cell in the computational mesh is used to form balances according to these five equations.

The general form of the continuity equation can be written as in Eqn. 2.1. When looking at 2D axisymmetric geometries, it is instead written as Eqn. 2.2.

$$\frac{\partial \rho}{\partial t} + \nabla \cdot (\rho \vec{v}) = 0 \tag{2.1}$$

$$\frac{\partial \rho}{\partial t} + \frac{\partial \rho}{\partial x}(\rho v_x) + \frac{\partial \rho}{\partial r}(\rho v_r) + \frac{\rho v_r}{r} = 0 \tag{2.2}$$

For an inertial, non-accelerating reference frame, conservation of momentum is described by Eqn. 2.3, where p is static pressure, $\bar{\bar{\tau}}$ is the stress tensor, $\rho\vec{g}$ is the gravitational body force, and $\vec{F}$ is the external body force. The equation for the stress tensor $\bar{\bar{\tau}}$ is described in Eqn. 2.4, where μ is molecular viscosity and I is the unit tensor.

$$\frac{\partial}{\partial t}(\rho\vec{v}) + \nabla \cdot (\rho\vec{v}\vec{v}) = -\nabla \cdot \rho + \nabla \cdot (\bar{\bar{\tau}}) + \rho\vec{g} + \vec{F} \tag{2.3}$$

$$\bar{\bar{\tau}} = \mu \left[\left(\nabla\vec{v} + \nabla\vec{v}^T \right) - \frac{2}{3}\nabla \cdot \vec{v} I \right] \tag{2.4}$$

The axial and radial momentum conservation equations for 2D axisymmetric geometries are given by Eqn. 2.5 and 2.6, respectively, where $\nabla \cdot \vec{v}$ is given by Eqn. 2.7.

$$\frac{\partial}{\partial t}(\rho v_x) + \frac{1}{r}\frac{\partial}{\partial x}(r\rho v_x v_x) + \frac{1}{r}\frac{\partial}{\partial r}(r\rho v_r v_x) = -\frac{\partial p}{\partial x} + \frac{1}{r}\frac{\partial}{\partial x}\left[r\mu \left(2\frac{\partial v_x}{\partial x} - \frac{2}{3}(\nabla \cdot \vec{v}) \right) \right] + \frac{1}{r}\frac{\partial}{\partial r}\left[r\mu \left(\frac{\partial v_x}{\partial x} + \frac{\partial v_r}{\partial x} \right) \right] + F_x \tag{2.5}$$

$$\frac{\partial}{\partial t}(\rho v_r) + \frac{1}{r}\frac{\partial}{\partial x}(r\rho v_x v_r) + \frac{1}{r}\frac{\partial}{\partial r}(r\rho v_r v_r) = -\frac{\partial p}{\partial r} + \frac{1}{r}\frac{\partial}{\partial x}\left[r\mu \left(\frac{\partial v_r}{\partial x} + \frac{\partial v_x}{\partial r} \right) \right] + \frac{1}{r}\frac{\partial}{\partial r}\left[r\mu \left(2\frac{\partial v_r}{\partial r} - \frac{2}{3}(\nabla \cdot \vec{v}) \right) \right] - 2\mu\frac{v_r}{r^2} + \frac{2}{3}\frac{\mu}{r}(\nabla \cdot \vec{v}) + \rho\frac{v_z^2}{r} + F_r \tag{2.6}$$

$$\nabla \cdot \vec{v} = \frac{\partial v_x}{\partial x} + \frac{\partial v_r}{\partial r} + \frac{v_r}{r} \tag{2.7}$$

2.2 Simulation Setup

The computational domain along with the assigned boundary conditions is shown in Fig. 2.2. Flow was simulated using a 2D axisymmetric solver. The inlet pressure, shown by the blue arrows, of the nozzles designed in this study were set to 4.0 MPa and 673

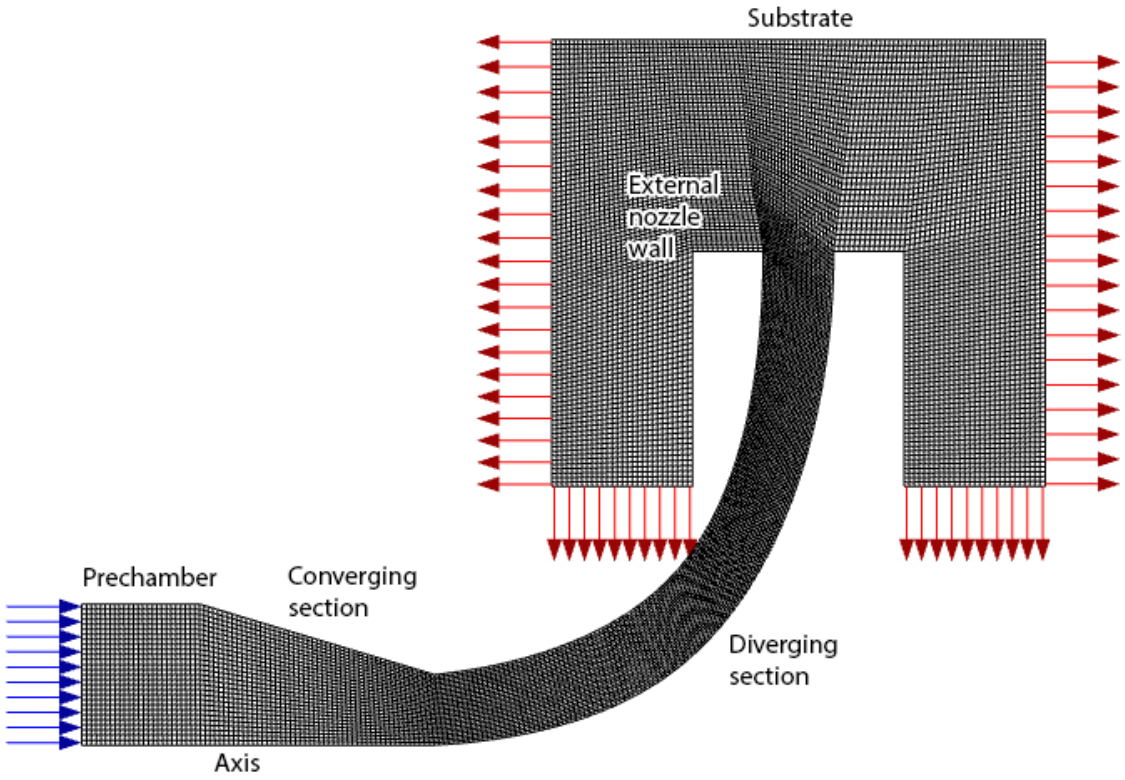

Figure 2.2 Radial cold spray nozzle design

K. The outlet pressures, shown by the red arrows, were set to the normal temperature and pressure (NTP) values of 101.325 kPa and 293 K. The axis, prechamber, converging section, diverging section, external nozzle wall, and substrate are all labeled. The upper horizontal line represents the substrate. The lower horizontal line is the nozzle axis.

Helium was used as the fluid, and its density was modeled using the ideal gas equation. Walls were assigned the no slip condition. Flow was assumed to be steady. Although density-based solvers are typically used for compressible flow simulations, a pressure-based solver was used instead. The SIMPLE pressure-velocity coupling model was used. Spatial discretization was set to first-order upwind with the least squares cell-based gradient evaluation. No wall heat transfer was modeled. Flow was modeled as either laminar or turbulent using the k-ϵ model.

The designs described by Kosarev et al. were recreated and tested according to their specified boundary conditions [29]. The inlets were set to two values of pressure, 1.5 MPa and 2.5 MPa, and two values of temperature, 300 K and 500 K. The outlets were set to NTP. The SST k-ω turbulence model was used.

When tangential velocities at the inlet were considered, the flow was simulated using

the axisymmetric swirl solver. Including simulations where there was assumed to be no swirl, three swirl angles were used in total: 0°, 15°, and 30°. Angles above 30° became unstable.

Chapter 3

Results and Discussion

The results of the simulations are discussed in this chapter. The nozzle design of Kosarev et al. is analyzed first, followed by discussion of two nozzles designed in this study.

3.1 Evaluation of Previous Nozzles

The nozzle designed by Kosarev et al. is an annular nozzle that features a central channel of constant area that makes a sharp 90° turn [29–31]. The flow then travels radially outwards from this contact point along the path of two flat plates. The distance between the plates is kept constant throughout the diverging section at a distance of 1 or 2 mm, depending on nozzle design.

A contour plot of the Mach number and the velocity streamlines of the Kosarev et al. 2 mm plate distance design is shown in Fig. 3.1. As seen in the figure, there is a sharp inner corner whose presence creates a stagnation point. The stagnation point causes the flow to separate, as indicated by the dark color. The particles gain radial momentum which increases their likelihood both of colliding with other particles and colliding with the nozzle wall. By gradually changing the curvature of this inner corner and the flow path, the flow separation can be averted, as seen in Fig. 3.2 which represents a design developed in this study.

As can be seen in Fig. 3.2, the Mach number contours of the fluid flow are more uniform across the nozzle cross-section when the sharp angle on the inner surface has been smoothed.A minor change to the original nozzle design of smoothing out the inner corner should help reduce particle collisions with the nozzle wall and as a result would

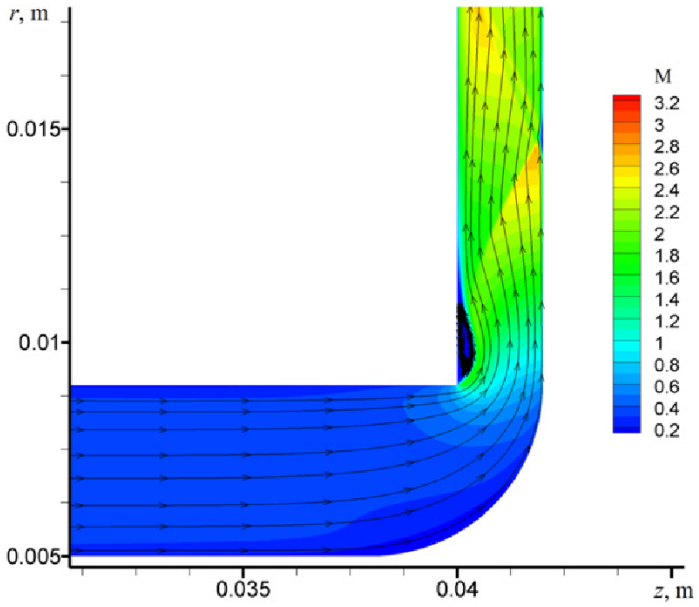

Figure 3.1 Mach number contours of the original radial nozzle design, figure from [29]. Note the sharp inner bend and dark patch representing flow separation.

reduce nozzle clogging. In addition, even with the design adjustment, the nozzle still features the same Mach ratio.

Oblique shocks off the nozzle walls were observed both in Kosarev's design and the adjusted design, as shown in Figs. 3.1 and 3.2, respectively. These oblique shocks reflect off the nozzle walls and can potentially destabilize the fluid flow, providing an additional risk of nozzle clogging.

Another notable feature of these nozzles is the sudden 90° turn of the flow path. As mentioned earlier, a large angle of bend increases the probability of the particles colliding against the nozzle wall. These collisions increase the chance of either nozzle clogging or wall erosion. However, in either of the outcomes, the impact velocity of the particle plays a significant role.

Kosarev et al. suggested that turning the flow early in the nozzle, before the particles have greatly accelerated, might prevent nozzle clogging since the fluid will still be moving at comparatively slow speeds [30]. However, if the particles are colliding against the wall at a speed below their critical velocities, they will cause the wall to erode. In either case, clogging or erosion will alter the shape of the channel, thereby affecting both the flow speed and direction. Even if operating under the assumption that neither clogging nor erosion are issues at the immediate nozzle bend, the particles' radial velocities still increase the likelihood of both particle-particle and particle-wall collisions later on in the

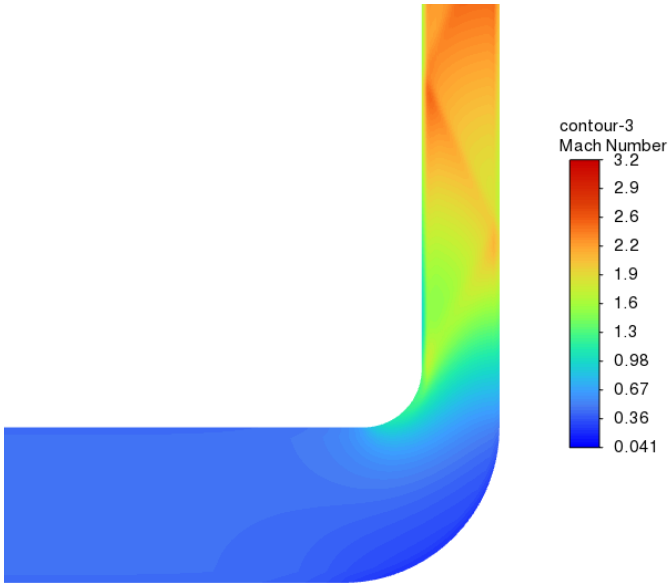

Figure 3.2 Mach number contours of the adjusted radial nozzle design. Note the gradual inner bend.

flow path.

To summarize, minimizing the flow separation required only a minor smoothing of the inner corner of the nozzle. However, modifying the bend angle requires a fundamental change to the nozzle design. This design modification and its outcomes are discussed in the following section.

3.2 New Nozzle Designs

A couple of nozzle designs featuring a gradual bend angle in comparison to the Kosarev nozzle are discussed in this section. Nozzle 1 features equidistant plate separation, as in the Kosarev nozzle, and a gradual bend angle. Nozzle 2 features a progressively shrinking plate separation and greater axial length compared to Nozzle 1.

3.2.1 Nozzle 1

The first nozzle design, depicted in Fig. 3.3, was constructed to have a more gradual bend angle than that seen in the Kosarev nozzles. It features a diverging section that gradually curves outwards as distance from the throat increases. Similar to the Kosarev nozzle, the distance between the two plates is kept roughly equivalent from the nozzle throat to the nozzle exit.

This design results in overexpanded flow, which is evident by the flow separation at the nozzle exit. It can be further observed that the fluid flow is pushed to the far wall, resulting in an uneven particle distribution on the substrate. The nozzle also shows the presence of an oblique shock along the walls of the nozzle and some reversed flow. Although powder particles were not simulated, it is evident by the velocity vectors in Fig. 3.3b that the flow gains additional radial velocity following the oblique shock. This would likewise impart additional radial velocities on the particles.

There are three types of nozzle expansion: optimal expansion, overexpansion, and underexpansion. By increasing the cross-sectional area of the nozzle through the diverging

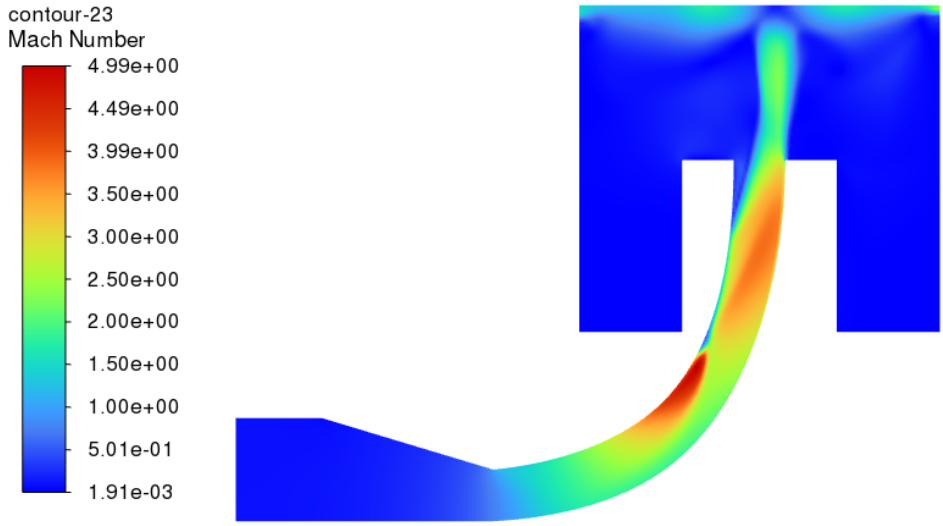

(a) Mach number

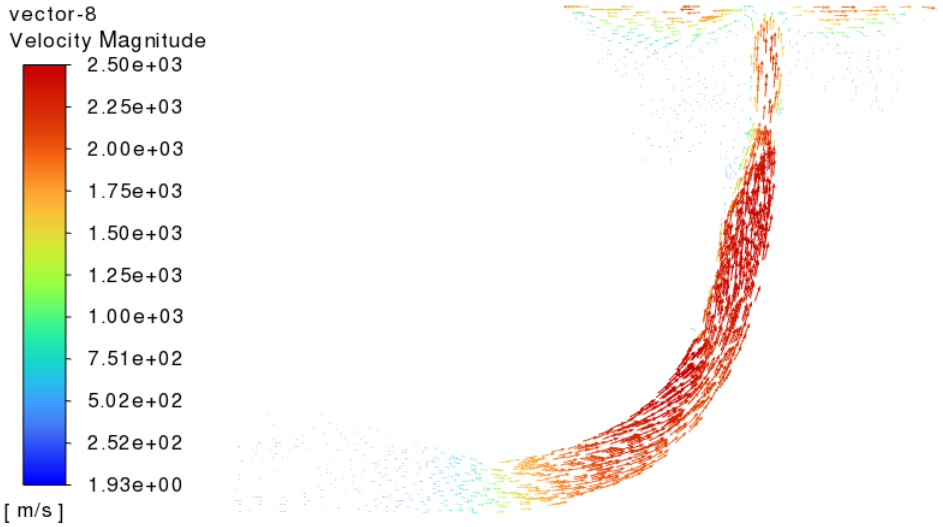

(b) Velocity vectors

Figure 3.3 Nozzle 1 Mach number and velocity.

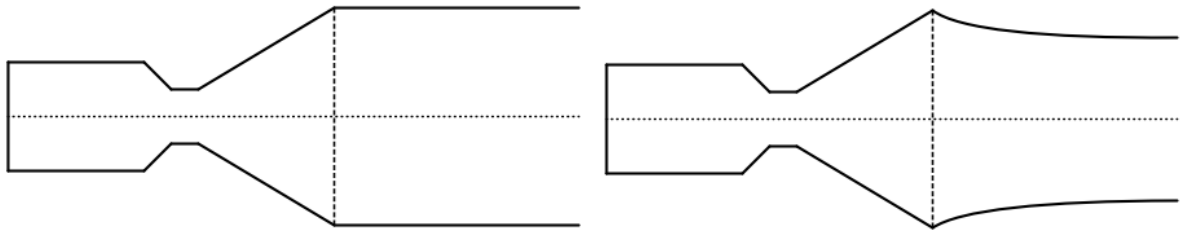

(a) Optimally expanded nozzle

(b) Overexpanded nozzle

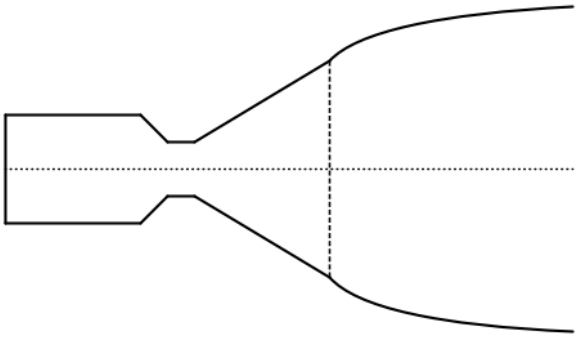

(c) Underexpanded nozzle

Figure 3.4 Types of nozzle expansion. The dotted line indicates the center axis. The dashed line indicates the nozzle exit.

section, the pressure of the fluid will decrease towards atmospheric conditions. If the pressure at the nozzle exit is below ambient pressure, it is considered overexpanded. An overexpanded nozzle has an exit area greater than the ideal case. Given a high enough difference between nozzle and atmospheric pressure, the flow separates at the exit. Conversely, if the nozzle pressure at the exit is above ambient pressure, it is considered underexpanded. An underexpanded nozzle has an exit area less than the ideal case. In an underexpanded nozzle, once exiting the nozzle into an area of lower pressure the fluid flow will increase in speed. An optimal nozzle design would be such that the exit and atmospheric pressures are equal. Otherwise, the nozzle will have a loss of efficiency. These three cases, optimal expansion, overexpansion, and underexpansion, are depicted in Fig. 3.4.

The ideal nozzle throat to nozzle outlet area ratio was calculated using Eqn. 3.1, where $A^\star$ is the area of the throat and A is the area of the nozzle outlet. The outlet area

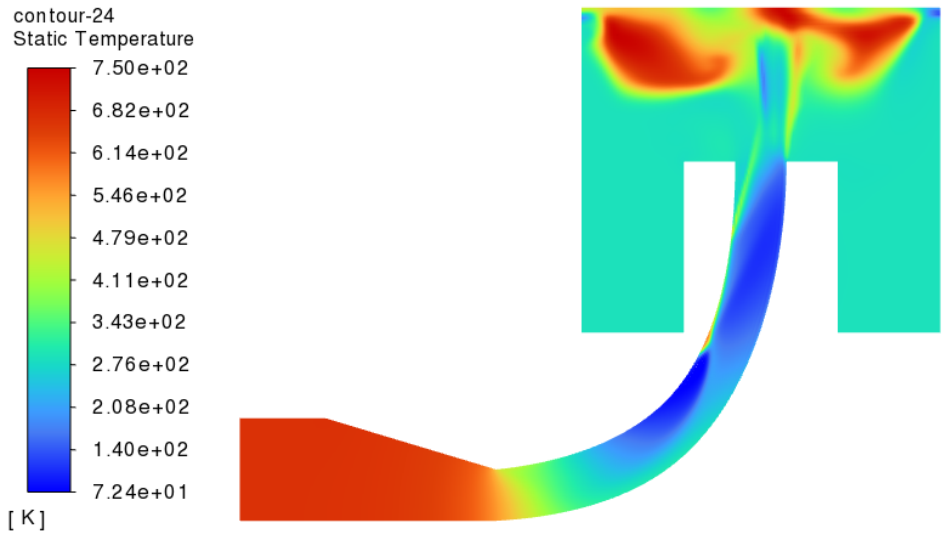

Figure 3.5 Nozzle 1 temperature distribution.

of Nozzle 1 was calculated to be almost double the ideal outlet area.

$$\frac{A^\star}{A} = \frac{\left(\frac{p}{p_t}\right)^{\frac{1}{\gamma}}\left[1-\left(\frac{p}{p_t}\right)^{\frac{\gamma-1}{\gamma}}\right]^{\frac{1}{2}}}{\left(\frac{\gamma-1}{2}\right)^{\frac{1}{2}}\left(\frac{2}{\gamma+1}\right)^{\frac{\gamma+1}{2(\gamma-1)}}} \tag{3.1}$$

The temperature profile is depicted in Fig. 3.5. There is a spike in temperature near the substrate. This apparent violation of conservation of energy equations implies that the simulation did not converge properly. The convergence criteria may have to be tightened to improve the results seen here. There may also have been an issue with the boundary conditions not considering reversed flow at the outlets.

One of the potential ways to mitigate the flow separation due to overexpansion is adding swirl to the flow. This was achieved by assigning a tangential velocity to flow at the nozzle inlet, which tends to push flow towards the outer edge. The swirl angle was set to 15° and 30°.

However, contrary to the expectation, the addition of swirl exacerbated the flow separation. With a 15° swirl angle, seen in Fig. 3.6 and 3.7, the flow is comparable to the flow when the tangential velocity component was set to 0. There are some additional oscillations in the free jet but similar levels of flow separation were observed. In the case of the 30° swirl angle, shown in Fig. 3.8 and 3.9, the flow separation becomes profound. The free jet also gets pushed to the far side of the nozzle, which would put a greater stress on that side and it is likely to increase particle collisions against the wall.

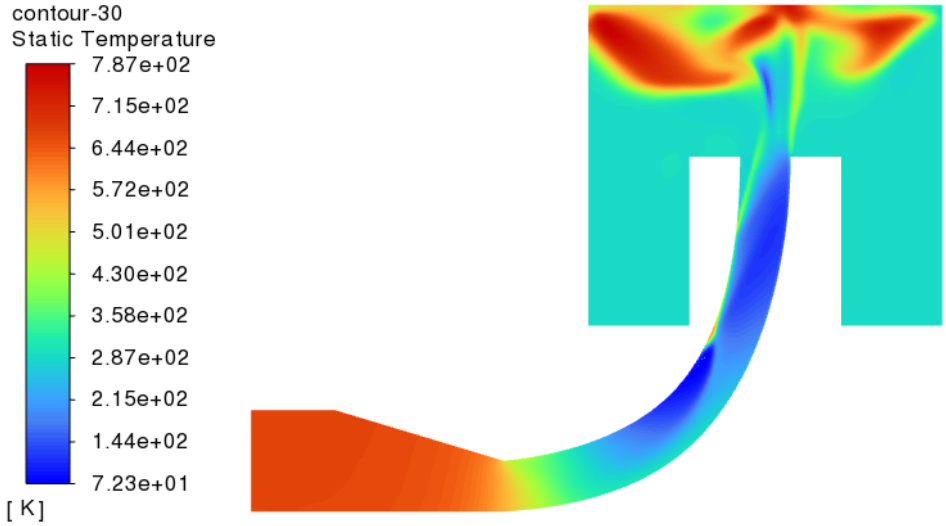

Figure 3.6 Nozzle 1 temperature with swirl angle of 15°.

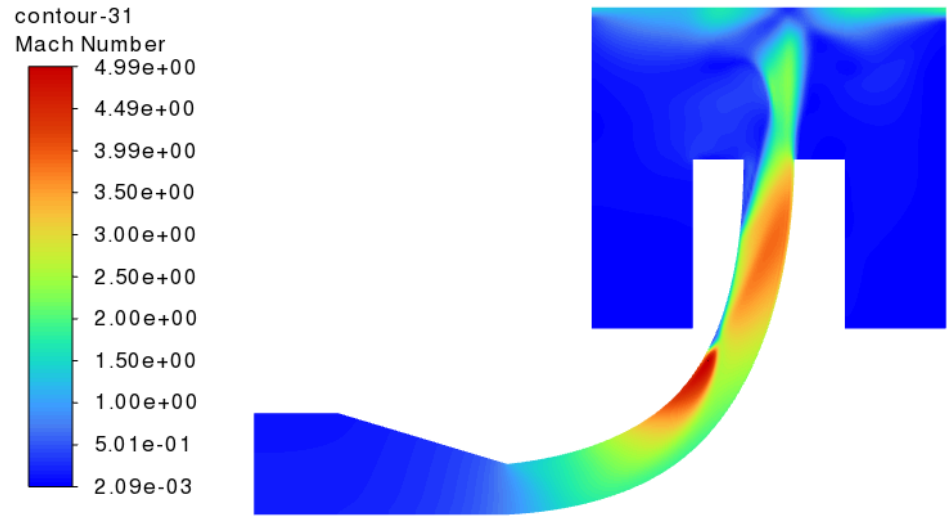

Figure 3.7 Nozzle 1 Mach number with swirl angle of 15°.

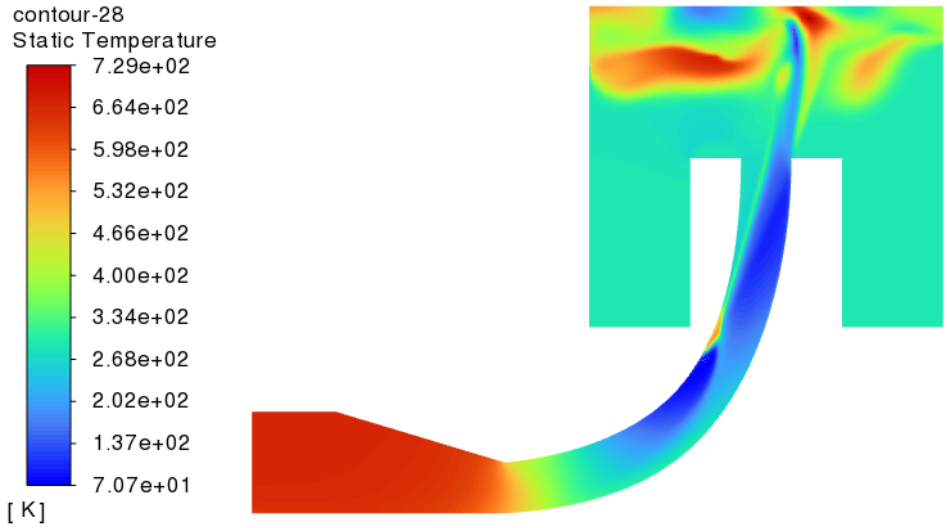

Figure 3.8 Nozzle 1 temperature with swirl angle of 30°.

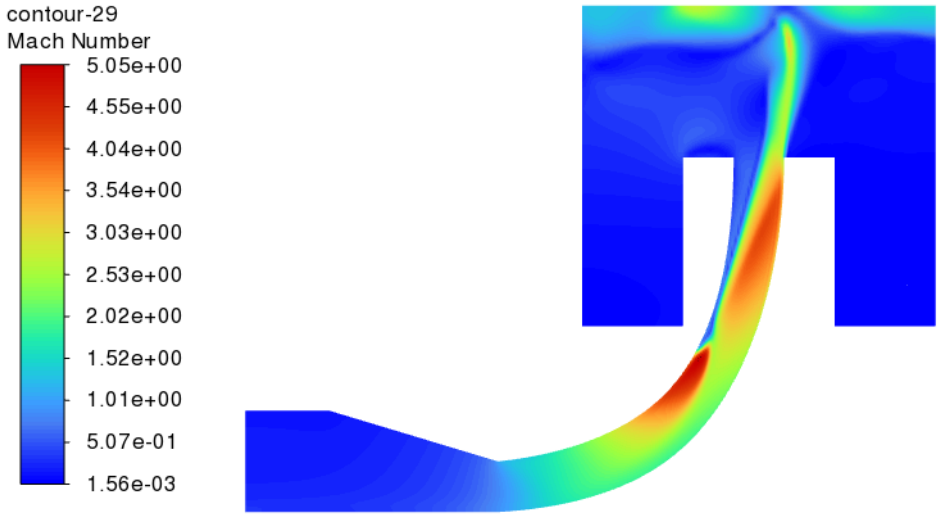

Figure 3.9 Nozzle 1 Mach number with swirl angle of 30°.

3.2.2 Nozzle 2

In order to alleviate the issues seen in Nozzle 1, the subsequent nozzle design depicted in Fig. 3.10 was developed. In this design, to provide a gradual increase in cross-sectional area, the length of the nozzle was increased along its axis of rotation. Furthermore, the outlet of the nozzle has also been narrowed. As a result, along the axis of the nozzle, the distance between the two plates decreases gradually in Nozzle 2 whereas the two plates were equidistant in Nozzle 1.

As shown in 3.10, the adjustments to the nozzle avoided the oblique shock observed in Nozzle 1 (Fig. 3.3). Additionally, it can be observed that this nozzle design results in an underexpanded flow, which can be seen by the sudden acceleration of fluid immediately upon exiting the nozzle.

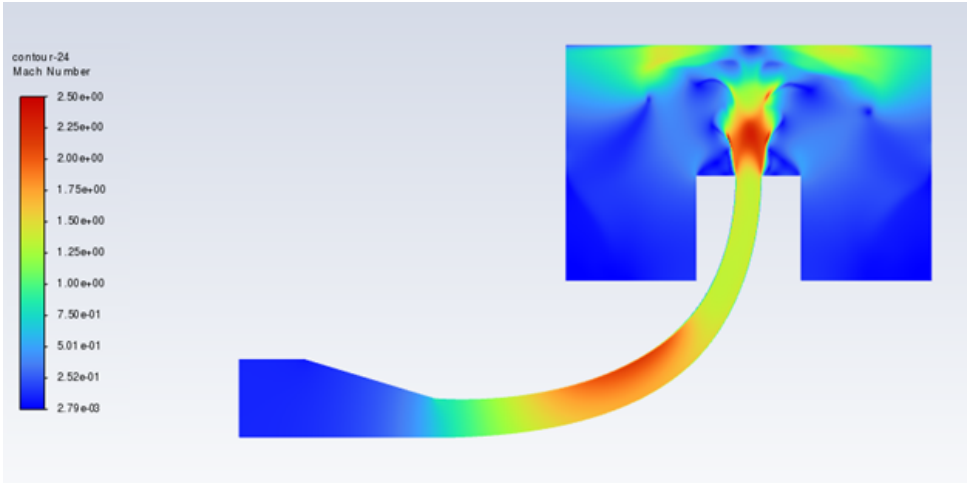

(a) Mach number

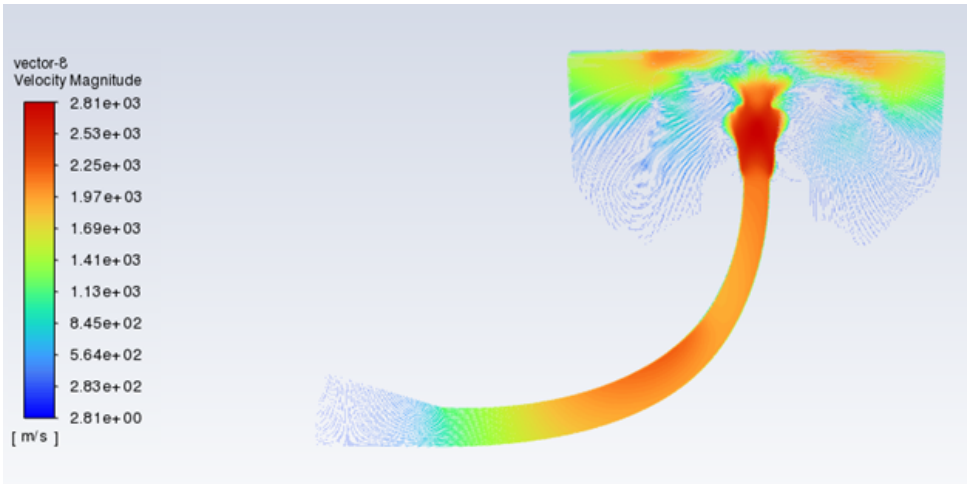

(b) Velocity

Figure 3.10 Nozzle 2 Mach number and velocity.

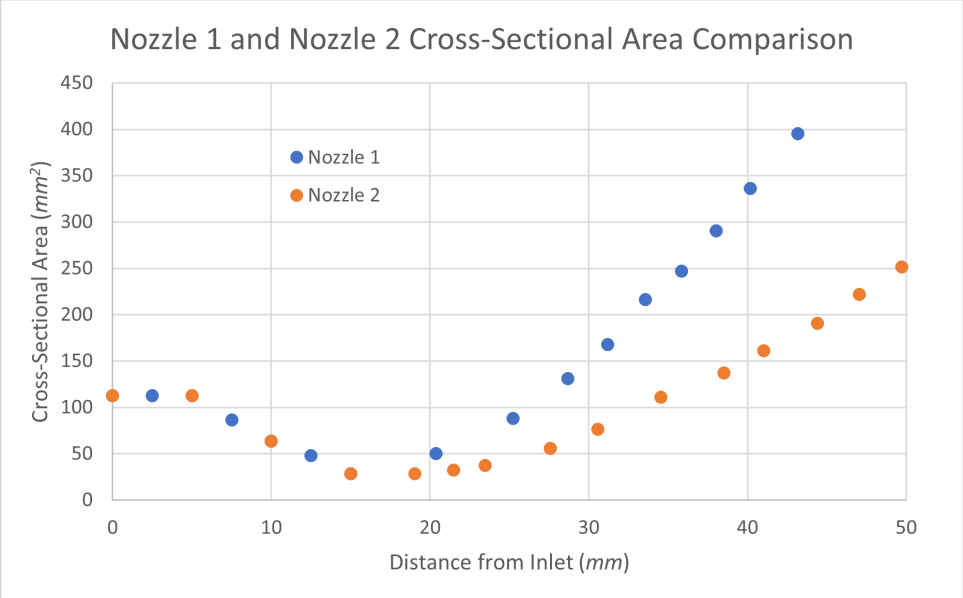

Figure 3.11 A comparison of the cross-sectional areas of Nozzle 1 and Nozzle 2, plotted against the distance from the nozzle inlet.

A comparison of the cross-sectional areas of Nozzle 1 and Nozzle 2 is given in Fig. 3.11. The equation for the surface area of a frustum, Eqn. 3.2, was used to calculate these areas. L is the slant height of the cone, r_1 is the radius of the large base or outer side of the nozzle, and r_2 is the radius of the small base or inner side of the nozzle. A figure illustrating this is given in the Appendix. L, r_1, and r_2 were measured by hand.

$$A_S = \pi L(r_1 + r_2) \tag{3.2}$$

The area of the prechamber and converging section of each nozzle was kept the same for consistency. Fig. 3.2 demonstrates that Nozzle 2 features a more gradual increase in corss-sectional area compared to Nozzle 1. Nozzle 1 features both a more rapid increase in area and a greater exit area than Nozzle 2. Additionally, Nozzle 2's diverging section cross-sectional area initially stays roughly constant with the area of the throat before beginning to increase. This has led to the nozzle throat, where Mach number equals 1, moving further downstream in Nozzle 1 compared to Nozzle 2 (see Fig. 3.3a and 3.10a).

Chapter 4

Conclusions

The primary concern with preexisting directional and radial cold spray nozzles was the drastic bend angle meant to accommodate smaller openings and repair sites. A large bend angle increases particle collisions with the nozzle wall since the flow cannot move as easily around the obstruction. Accordingly, this increases the risk of clogging and erosion, depending on the location of the bend. Both of these concerns depend on particle velocity; namely, they depend on whether the particles have managed to accelerate above their critical velocity or not, respectively. Nozzle clogging and erosion change the shape of the channel, affecting particle velocity and direction and impairing the particles' ability to impinge on the substrate.

While nozzle clogging is a risk in any cold spray nozzle, it is of particular concern in bent cold spray nozzles due to the increased likelihood of particles impacting on the nozzle wall.

It is proposed that a more gradual bend of the nozzle channel will help avoid major clogging or erosion issues, since the fluid will more easily be able to flow through the nozzle without particles impacting on the interior wall. Although no ideal nozzle design has been found, adjustments to a previous nozzle designed by Kosarev et al. to smooth out a sharp corner on the internal nozzle walls have been found to reduce flow separation with no loss in Mach number.

Flow separation is a primary concern with these nozzle designs since it imparts secondary velocities on the flow that increases the likelihood of particle collisions with the nozzle wall. Both the original Kosarev nozzles and one of the nozzles designed in this study, Nozzle 1, exhibit flow separation. By reducing flow separation, the nozzle will be less likely to clog due to the fewer number of collisions occurring.

Limitations to this thesis include assuming single-phase flow in the simulation rather than multi-phase flow with particles. Simulating multi-phase flow would show the particle movement in addition to the flow of the carrier gas. Additionally, one of the nozzles failed to converge properly. This could be due to an issue with the convergence criteria or with the boundary conditions.

References

(1) Monette, Z.; Kasar, A. K.; Daroonparvar, M.; Menezes, P. L. *The International Journal of Advanced Manufacturing Technology* **2020**, *106*, 2079–2099.

(2) Jones, R.; Matthews, N.; Rodopoulos, C. A.; Cairns, K.; Pitt, S. *International Journal of Fatigue* **2011**, *33*, 1257–1267.

(3) Lee, J.; Kang, H.; Chu, W.; Ahn, S. *CIRP Annals* **2007**, *56*, 577–580.

(4) Jr, V. C.; Kaplowitz, D.; III, V. K. C.; Howe, C.; West, M. K.; McNally, B.; Rokni, M. *Materials and Manufacturing Processes* **2018**, *33*, 130–139.

(5) Yin, S.; Cavaliere, P.; Aldwell, B.; Jenkins, R.; Liao, H.; Li, W.; Lupoi, R. *Additive Manufacturing* **2018**, *21*, 628–650.

(6) Ozdemir, O. C.; Widener, C. A.; Helfritch, D.; Delfanian, F. *Journal of Thermal Spray Technology* **2016**, *25*, 660–671.

(7) Foelsche, A. Nozzle Clogging Prevention and Analysis in Cold Spray, Ph.D. Thesis, University of Massachusetts Amherst, 2020.

(8) Kosarev, V. F.; Klinkov, S. V.; Alkhimov, A. P.; Papyrin, A. N. *Journal of Thermal Spray Technology* **2003**, *12*, 265–281.

(9) Raletz, F.; Vardelle, M.; Ezo'o, G. *Surface and Coatings Technology* **2006**, *201*, 1942–1947.

(10) Palodhi, L.; Singh, H. *Journal of Thermal Spray Technology* **2020**, *29*, 1863–1875.

(11) Wang, Z.; Cai, S.; Chen, W.; Ali, R. A.; Jin, K. *Journal of Thermal Spray Technology* **2021**, *30*, 1213–1225.

(12) Li, W.; Li, C.-J. *Journal of Thermal Spray Technology* **2005**, *14*, 391–396.

(13) Li, C.-J.; Li, W.-Y.; Liao, H. *Journal of Thermal Spray Technology* **2006**, *15*, 212–222.

(14) Assadi, H.; Gärtner, F.; Stoltenhoff, T.; Kreye, H. *Acta Materialia* **2003**, *51*, 4379–4394.

(15) Grujicic, M.; Zhao, C. L.; DeRosset, W. S.; Helfritch, D. *Materials & Design* **2004**, *25*, 681–688.

(16) Hassani-Gangaraj, M.; Veysset, D.; Champagne, V. K.; Nelson, K. A.; Schuh, C. A. *Acta Materialia* **2018**, *158*, 430–439.

(17) Champagne, V. K.; Helfritch, D. J.; Dinavahi, S. P. G.; Leyman, P. F. *Journal of Thermal Spray Technology* **2011**, *20*, 425–431.

(18) Gärtner, F.; Stoltenhoff, T.; Schmidt, T.; Kreye, H. *Journal of Thermal Spray Technology* **2006**, *15*, 223–232.

(19) Sakaki, K. In *Designing, Processing and Properties of Advanced Engineering Materials*, Trans Tech Publications Ltd: 2004; Vol. 449, pp 1305–1308.

(20) Alexandre, S.; Laguionie, T.; Baccaud, B. In *Thermal Spray 2007: Global Coating Solutions: Proceedings of the 2007 International Thermal Spray Conference*, Google-Books-ID: CwbFg2Nk98IC; ASM International: 2007, pp 1–6.

(21) Varadaraajan, V.; Mohanty, P. *Surface and Coatings Technology* **2017**, *316*, 246–254.

(22) Sakaki, K. In *Cold Gas Dynamic Spray*; CRC Press: 2016, pp 95–118.

(23) Santos da Silva, F.; Cinca i Luis, N.; Dosta Parras, S.; García Cano, I.; Guilemany, J. M. (M.; Benedetti, A. V. **2017**, Accepted: 2020-04-28T07:51:27Z Publisher: Universidade Estadual Paulista.

(24) Li, W.-Y.; Liao, H.; Wang, H.-T.; Li, C.-J.; Zhang, G.; Coddet, C. *Applied Surface Science* **2006**, *253*, 708–713.

(25) Widener, C. A.; Carter, M. J.; Ozdemir, O. C.; Hrabe, R. H.; Hoiland, B.; Stamey, T. E.; Champagne, V. K.; Eden, T. J. *Journal of Thermal Spray Technology* **2016**, *25*, 193–201.

(26) Hoiland, B.; Schell, J.; Howe, C. Directional cold spray method, 2018.

(27) Payne, D. A. Apparatus for applying cold-spray to small diameter bores, en, 2011.

(28) Huber, H.; Vlcek, J.; Voggenreiter, H. Fixed inner spray nozzle to supply gas and powder mixture, for painting surfaces, has sleeve and insert, formed so that outer contour of insert forms Laval nozzle with inner contour of sleeve, IPC:

(29) Kiselev, S. P.; Kiselev, V. P.; Klinkov, S. V.; Kosarev, V. F.; Zaikovskii, V. N. *Surface and Coatings Technology* **2017**, *313*, 24–30.

(30) Kosarev, V. F.; Klinkov, S. V.; Zaikovskii, V. N.; Kundasev, S. G. *Thermophysics and Aeromechanics* **2015**, *22*, 667–676.

(31) Kosarev, V. F.; Klinkov, S. V.; Zaikovskii, V. N. *Thermophysics and Aeromechanics* **2016**, *23*, 311–318.

(32) Kiselev, S. P.; Kiselev, V. P.; Zaikovskii, V. N. **2019**, *1268*, Publisher: IOP Publishing, 012033.

(33) Klinkov, S. V.; Kosarev, V. F.; Zaikovskii, V. N. *Surface Engineering* **2016**, *32*, Publisher: Taylor & Francis _eprint: https://doi.org/10.1179/1743294415Y.0000000070, 701–706.

(34) Horlock, J. H.; Lakshminarayana, B. *Annual Review of Fluid Mechanics* **1973**, *5*, 247–280.

(35) Detra, R. W. The secondary flow in curved pipes, en, Ph.D. Thesis, ETH Zurich, 1953.

(36) Cuming, H. G. *Aeronautical Research Council Reports & Memoranda* **1952**, *2880*, Accepted: 2014-10-21T15:53:21Z.

(37) Stanitz, J. D.; Osborn, W. M.; Mizisin, J. *3015* **1953**, Number: NACA-TN-3015.

(38) Suryan, A.; Ephram, S.; Nair, P. P.; Kim, H. D. *AIP Conference Proceedings* **2019**, *2134*, Publisher: American Institute of Physics, 040007.

(39) Briley, W. R.; Mcdonald, H. *Journal of Fluid Mechanics* **1984**, *144*, Publisher: Cambridge University Press, 47–77.

(40) Baker, T. J. Fluent User's Guide, English, 2020.

(41) Fusion 360, online, 2022.

(42) Versteeg, H. K.; Malalasekera, W., *An Introduction to Computational Fluid Dynamics: The Finite Volume Method*; Pearson Education Limited: 2007.

(43) Sabrowski Pierre, G. T. Computational Fluid Dynamics Methods Explained.

(44) Maev, R. G.; Leshchynsky, V., *Cold Gas Dynamic Spray*, Google-Books-ID: 070ODAAAQBAJ; CRC Press: 2016.

(45) Alkhimov, A. P.; Papyrin, A. N.; Kosarev, V. F.; Nesterovich, N. I.; Shushpanov, M. M. Gas-dynamic spraying method for applying a coating, 1994.

(46) Yin, S.; Chen, C.; Suo, X.; Lupoi, R. *Advances in Materials Science and Engineering* **2018**, *2018*, ed. by Bondioli, F., Publisher: Hindawi, 2804576.

(47) Surface Area of Frustum, en.

Appendix A

Supplementary Figures

Surface Area of Frustum of a Cone Formulas

cuemath
THE MATH EXPERT

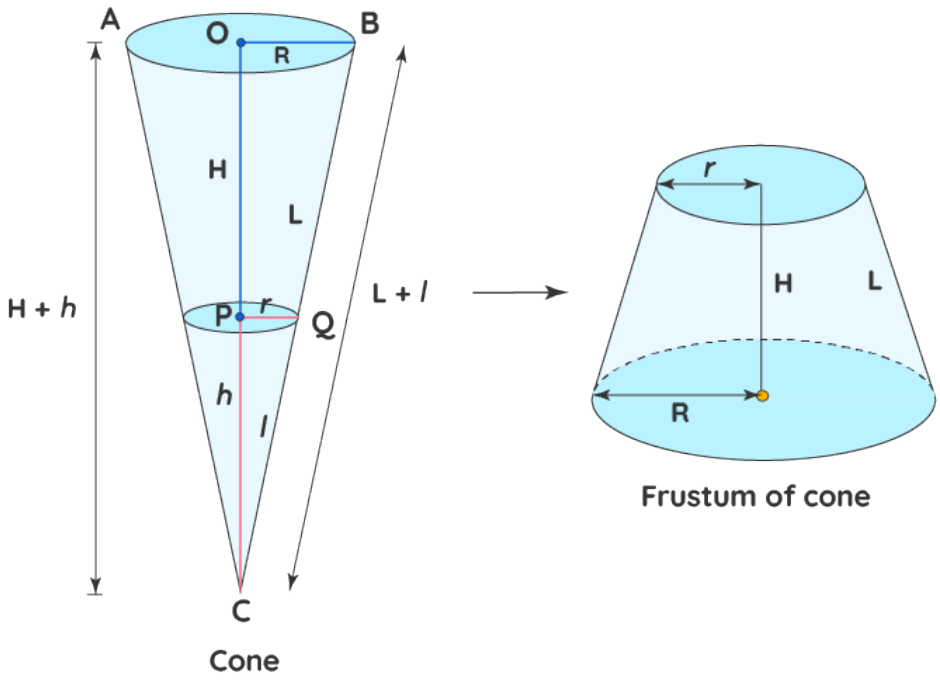

CSA of frustum = $\pi l\left(\frac{R^2 - r^2}{r}\right)$ OR $\pi L(R + r)$

TSA of frustum = $\pi l\left(\frac{R^2 - r^2}{r}\right) + \pi(R^2 + r^2)$

OR

$\pi L(R + r) + \pi(R^2 + r^2)$

Note : $L^2 = H^2 + (R - r)^2$

Figure A.1 Formulas to calculate the surface area of a frustum of a cone [47]. CSA refers to the curved surface area. TSA refers to the total surface area.

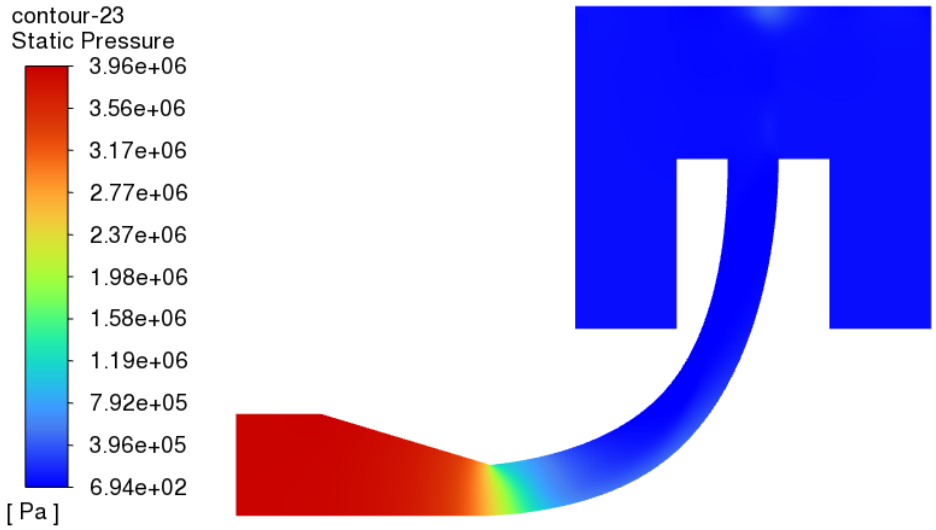

Figure A.2 Nozzle 1 pressure distribution.

Figure A.3 Nozzle 1 density distribution.

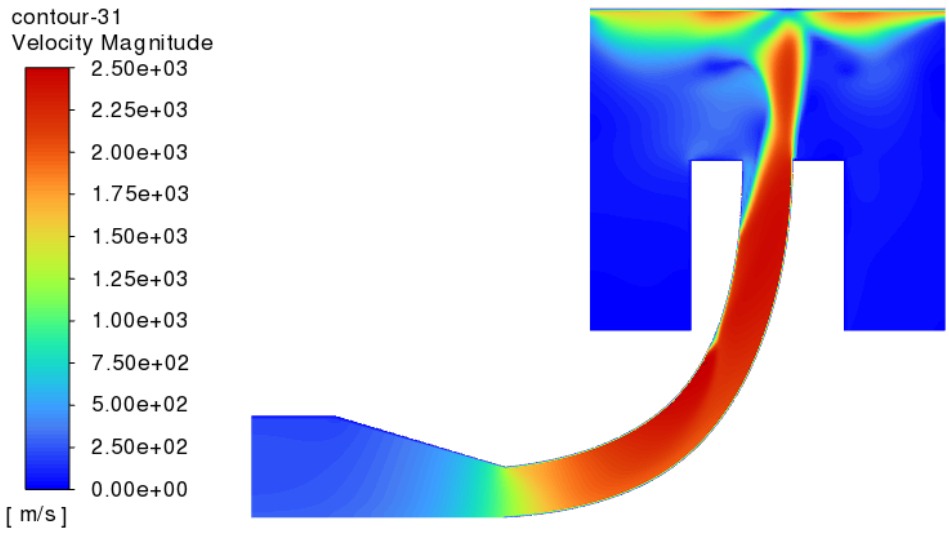

Figure A.4 Nozzle 1 velocity magnitude with swirl angle of 15°.

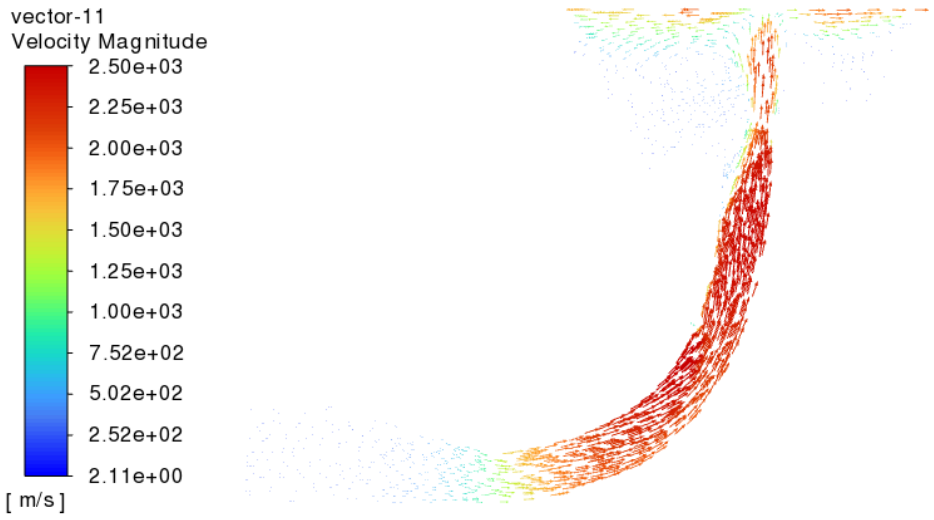

Figure A.5 Nozzle 1 velocity vectors with swirl angle of 15°.

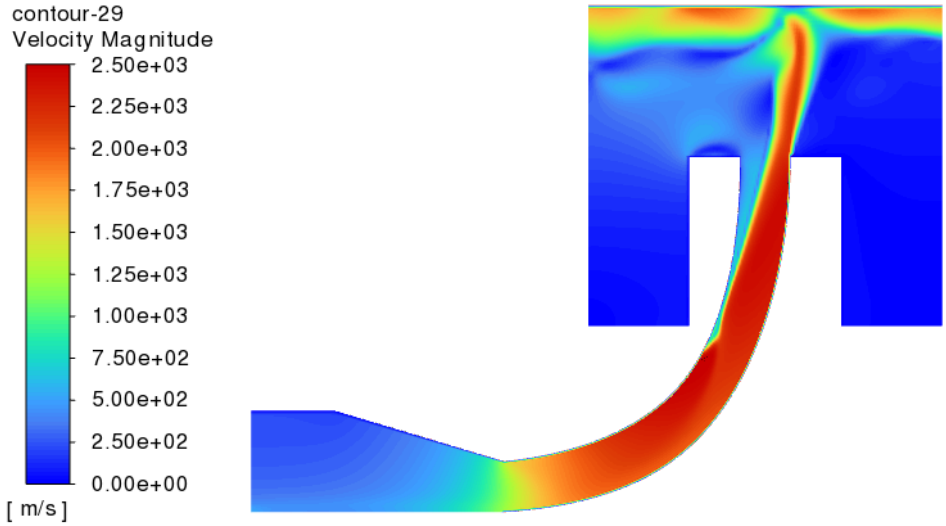

Figure A.6 Nozzle 1 velocity magnitude with swirl angle of 30°.

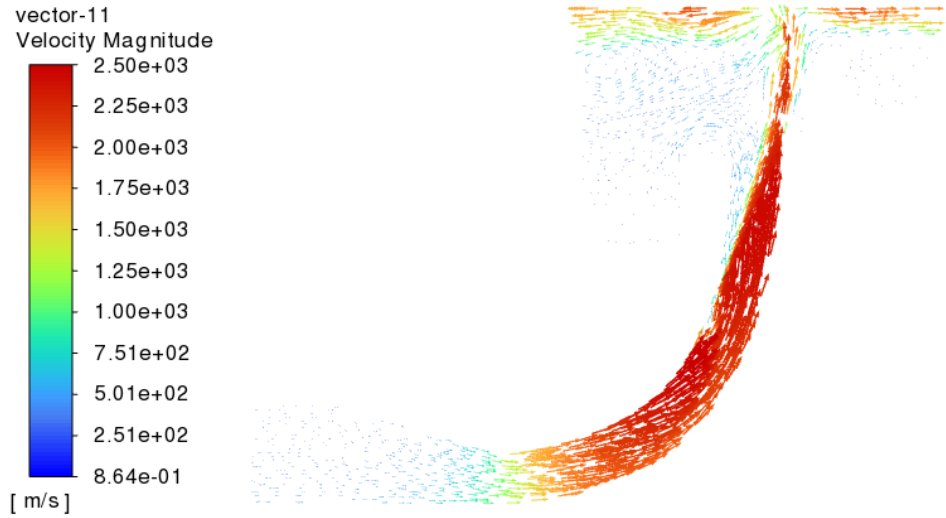

Figure A.7 Nozzle 1 velocity vectors with swirl angle of 30°.

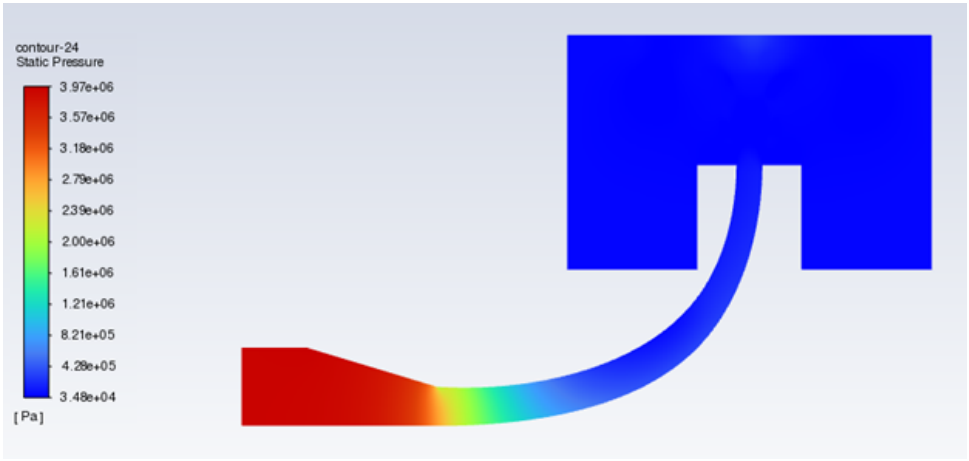

Figure A.8 Nozzle 2 pressure distribution.

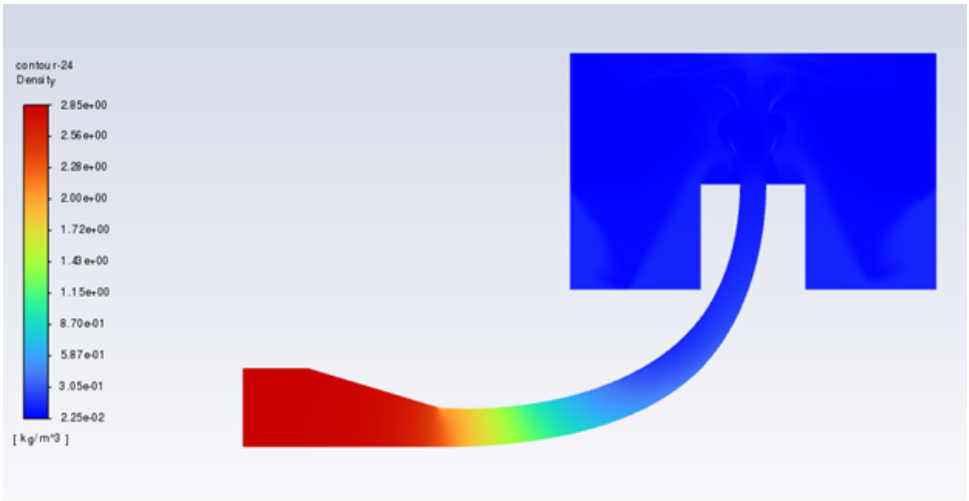

Figure A.9 Nozzle 2 density distribution.

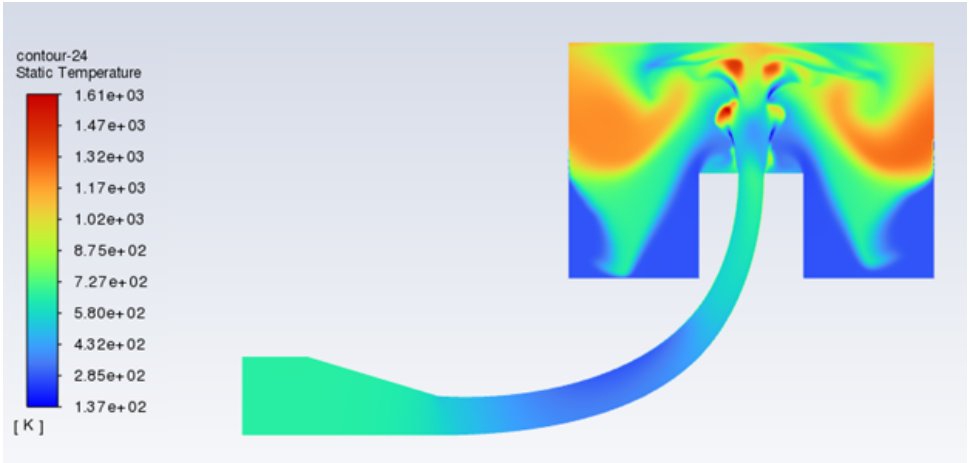

Figure A.10 Nozzle 2 temperature distribution.